LAWRENCE
LIVERMORE
NATIONAL
LABORATORY

UCRL-CONF-236386

Scaling Extreme Astrophysical Phenomena to the Laboratory

B. A. Remington

November 8, 2007

49th Annual Meeting of the Division of Plasma Physics
Orlando, FL, United States
November 12, 2007 through November 16, 2007

Disclaimer

Scaling extreme astrophysical phenomena to the laboratory*

Bruce A. Remington

Lawrence Livermore National Laboratory, USA

(Oct. 31, 2007, 10:20 pm)

ABSTRACT

High-energy-density (HED) physics refers broadly to the study of macroscopic collections of matter under extreme conditions of temperature and density. The experimental facilities most widely used for these studies are high-power lasers and magnetic-pinch generators. The HED physics pursued on these facilities is still in its infancy, yet new regimes of experimental science are emerging. Examples from astrophysics include work relevant to planetary interiors, supernovae, astrophysical jets, and accreting compact objects (such as neutron stars and black holes). In this paper, we review a selection of recent results in this new field of HED laboratory astrophysics and provide a brief look ahead to the coming decade.

I. INTRODUCTION

Modern high power lasers and magnetic pinch facilities produce energy densities in millimeter-scale volumes large enough to access phenomena that otherwise appear only in energetic astrophysical systems. Examples of areas that can be studied include strong shock phenomena; high Mach number jets; strongly coupled plasmas; compressible hydrodynamic instabilities; radiation flow; photoevaporation front hydrodynamics; and fundamental properties such as opacities and equations of state. [Remington 1999, 2000; Takabe, 2001]. Consequently, a new field of research is

emerging – high energy density laboratory astrophysics. [HEDLA-2004, 2005] We present a brief review of the emerging field of high energy density (HED) laboratory astrophysics, selecting experiments relevant to stellar interiors (Sec. II), planetary interiors (Sec. III), core-collapse supernova explosion hydrodynamics (Sec. IV), accretion disk photoionized plasmas (Sec. V), and relativistic collisionless plasma dynamics relevant to gamma-ray burst specctra (Sec. VI).

II. STELLAR INTERIORS

We start with a discussion of stellar interior dynamics and opacity measurements. A diagram of the ratio of the first two harmonics periods of a beat Cepheid variable star is shown in Fig. 1a. The upper set of three dashed curves correspond to the simulated result using older opacities, which ignore the full fine structure of the metals. The lower solid curves correspond to simulations with OPAL-DTA, including the full fine structure, in particular, for Fe. [Rogers and Iglesias, 1994.] The relevant density and temperature regime is illusrated by the schematic in Fig. 1b showing approximately the density and temperature of the interior of the sun, as a function of the normalized radius. [Rose, 2005] An experiment is under development on the Z magnetic pinch facility to measure the opacity of Fe under conditions relevant to the solar interior. A schematic diagram of the experiment is shown in Fig. 1c, along with an example space-resolved "raw" spectrum from one of the experiments. [Bailey, 2007] (d) Calculations of the expected Fe spectrum, compared to the Fe spectrum for the relevant conditions in the solar interior, are shown in Fig. 1d. The calculation shown in red corresponds to conditions at the radiation- convection boundary in the sun, and the plot in green to the conditions in Z

experiments. The Planck function derivative with respect to temperature evaluated at 180 eV (black) illustrates the photon energies most important for the solar radiation transport. [Bailey, 2007]

III. PLANETARY INTERIORS

The interior structure of the giant planets of our solar system (Jupiter, Saturn, Uranus, and Neptune) is determined by the compressibility of their constituent matter under the very high pressures due to the inwardly directed force of gravity. [Guillot, 1999] In laboratory terms, this compressibility is determined by the equation of state (EOS) of the constituent matter along an isentrope [Saumon 2004]. The EOS and other properties of matter at the extreme pressures and densities found in the interiors of the giant planets, however, are quite uncertain. The pressures of interest along an isentrope range from 1-70 Mbar in Jupiter, [Guillot 1999; Guillot, 2004] as shown for Jupiter in Fig. 2a. Characteristic isentropes for the giant planets indicate that the plasma in their interiors is both strongly coupled [$\Gamma = (Ze)^2/aT > 1$, where Z, e, a, and T correspond to ionization state, electron charge, average atomic spacing, and temperature (in units of energy)] and degenerate ($T/\varepsilon_F < 1$, where ε_F is the Fermi energy). [Van Horn, 1991] Hence, the internal structure, $\rho(r)$, $T(r)$, of the giant planets is determined by the EOS of dense, degenerate, strongly coupled plasmas and plasma mixtures at very high pressures, P = 1 to 40 Mbar, and moderate temperatures, kT < ~1 eV. The compressibility of hydrogen along a high pressure isentrope, and the predicted phase separation in a He-H mixture when hydrogen transitions to a metallic state are of central interest, both for the giant planets of our solar system, and for models of the extrasolar planets. [Fortney, 2004]

The interior structure of Jupiter is sensitive to the high pressure, high density properties of hydrogen. A schematic of the interior of Jupiter is shown in Fig. 2a. [Guillot, 2004.]

The simulated internal structure of the newly discovered, exo-planet, GJ 876d, is shown in Fig. 2b. This planet corresponds to one of the newly discovered "super-Earths", as it is thought to have nearly ten times the mass of the earth, but is still thought to be a terrestrial planet. Four different compositions are illustrated in Fig. 2b. The solid lines show the cases in which the composition of the core is taken to be pure Fe; dashed lines are for the case of $Fe_{0.2}(FeS)_{0.8}$. Lines with stars show the internal structure of GJ 876d if the composition is Earth-like. Squares show the density profile if this planet has 80% of the mass in the core. Circles show the structure if the planet had retained 20% of its mass as a water /ice layer. Diamonds show the density structure if GJ 876d retained 40% of water /ice. The Preliminary Reference Earth Model [PREM; Dziewonski & Anderson 1981] is shown for reference. [Valencia et al., Ap. J. 656, 545 (2007)]

Laboratory measurements of shock-free loading of aluminum to P_{max} = 2 Mbar has been developed in an experiment developed on the Omega laser (Fig. 2c). Particle velocity (lower curve) at the Al-LiF interface and extracted pressure (upper curve) at the front of the Al sample taken from the VISAR record. Heavy solid lines show velocity and extracted pressure averaged over 300 μm. Shading shows error bars generated from a spatial analysis of six velocity records e one taken every 50 pixels. Shading represents 90% confidence limits for both particle velocity and pressure. Over the peak drive window (t = 20-30 ns), the average deviation in particle velocity and pressure are 3.6% and 5.5%, respectively. [Lorenz, 2006]

III. SUPERNOVAE

Core-collapse supernovae result from the death of a massive star. Large stars have high enough temperatures in their cores to continue the nuclear fusion burning cycle up to Fe. Once the core reaches Fe, the nuclear fusion reactions no longer release net energy, and the thermonuclear fires are extinguished. At this point, there is no longer sufficient heat produced in the core to balance cooling by neutrino emission and photonuclear dissociation, and the core collapses under the force of gravity, triggering a catastrophic gravitational implosion that is over in a matter of seconds. This collapse is stopped only when the core density reaches that of degenerate nuclear matter (~2 x 10^{14} g/cm^3). The Fermi degeneracy pressure, $P_{deg} \sim \rho^{2/3}$, increases sufficiently to stop the implosion, and a spectacular nuclear rebound occurs whose strength is determined by the EOS of bulk nuclear matter. By a mechanism still debated, this launches a powerful outward-propagating shock that eventually blows the star apart. This explosive birth is observed as a bright flash of UV light, followed by an extended period of enormous luminosity. If the core has a mass larger than 2-3M_{sun}, the core collapse continues to form a black hole, otherwise a neutron star is formed.

Once the core rebound shock gets launched, a number of nonlinear hydrodynamic effects are initiated. During the shock transit phase, the Richtmyer-Meshkov (RM) instability is triggered at each discontinuity in the density profile of the star, i.e., at the O-He and He-H "interfaces." After shock transit, hydrodynamic mixing continues due to the Rayleigh-Taylor (RT) instability, as the denser layers are decelerated by the lower-density outer layers. Large-scale, two-dimensional calculations of the development of

the mixing at the O-He and He-H interfaces [Kifonidis, 2006] show that spikes of dense, iron- and Ni-rich core material penetrate outward into the less dense envelope of hydrogen, but are slowed down abruptly by the reverse shock near the H/He boundary (Fig. 3a-c). This interpenetration occurs through the growth and nonlinear evolution of the Rayleigh-Taylor (RT) instability.

Laser-based experiments can generate strong-shock induced nonlinear hydrodynamic mixing similar to those found in SNe. In a set of experiments scaled to approximately reproduce the gross hydrodynamics of the He-H interface of SN1987A about an hour after explosion, a strong shock was passed through an interface separating dense "core" material [CH(4% Br)] from the lower density outer envelope (CRF foam). [Miles, 2004] A single-mode ripple was imposed at the interface. The subsequent growth due to the RM and RT instabilities was measured by x-ray backlighting. Spikes of CH(Br) penetrating upward into less-dense CH_2 as a consequence of the Rayleigh-Taylor instability were experimentally observed at 13, 25, and 37 ns, as shown in Figs. 3d-f. The final image shows what appears to be a transition to turbulence, and affect not seen in the supernova simulations.

A theoretical look at the relation between the hydrodynamics occurring in the SN versus in the laboratory experiment shows that a rigorous mapping exists. In both settings, the Reynold's number (the ratio of the inertial to the viscous force) and the Peclet number (the ratio of the convective to the conductive heat transport) are large. Therefore, viscosity and thermal diffusivity are negligible, and the dynamics of the interface are well described by Euler's equations for a polytropic gas [Ryutov, 1999; 2000; 2001],

$$\rho\left(\frac{\partial \mathbf{v}}{\partial t}+\mathbf{v}\cdot\nabla\mathbf{v}\right)=-\nabla p \ ,$$

$$\frac{\partial \rho}{\partial t}+\nabla\cdot(\rho\mathbf{v})=0 \quad , \quad \text{and}$$

$$\frac{\partial p}{\partial t}-\gamma\frac{p}{\rho}\frac{\partial \rho}{\partial t}+\mathbf{v}\cdot\nabla p-\gamma\frac{p}{\rho}\mathbf{v}\cdot\nabla\rho=0 \quad , \qquad (1)$$

which represent conservation of momentum, mass, and entropy, respectively. It is straight-forward to show by substitution that Eq. 1 is invarient under the following scale transformation,

$$h_{SN} \rightarrow a h_{lab}, \qquad (2)$$

$$\rho_{SN} \rightarrow b\rho_{lab},$$

$$p_{SN} \rightarrow c p_{lab},$$

$$\tau_{SN} \rightarrow a(b/c)^{1/2}\tau_{lab},$$

where h, ρ, p, and τ correspond to characteristic spatial, density, pressure, and time scales, and subscripts *SN* and *lab* refer to the supernova and laboratory laser experiment, respectively. When transformation (2) is inserted into Eq. (1), the constants a, b, and c cancel, and the dynamics described by Euler's equation are indistinguishable in the SN and the laser experiment. Both settings are probing the same physics. Any insights gained through the laser experiment apply directly to the SN through the mapping described by Eq. 2. For example, the hydrodynamics illustrated in Figs. 2b and 2c are

similar, at least for some time interval, and can be related through the SN-to-laboratory mapping of h, ρ, p, τ, and $g= \nabla p/\rho$, given by Eq. 2. [Ryutov, 1999]

IV. ACCRETION DISK PHOTOIONIZED PLASMAS

One of the most intriguing objects in the universe is an accreting compact object, such as a neutron star or black hole. At the extreme is an accretion disk around a massive black hole (10^8-10^9 M_{sun}) at the center of a galaxy such as the active galactic nucleus (AGN) object NGC 4261. [Ferrarese, 1996] Another much closer example is Cyg X-3, an accreting x-ray binary system, illustrated schematically by the artistic sketch in Fig. 4a. An example spectrum from this accreting binary x-ray source Cyg X-3 is shown in Fig. 4b. [Paerels, 2000] These spectra result from the final plunge of matter from the accretion disk into the compact object, and have been shown to result from a photoionized plasma. In this case, radiative excitation, absorption, and emission processes dominate, and collisional processes are negligible. The emission-line spectrum of the X-ray binary Cygnus X-3 is consistent with recombination-dominated line formation. From this it is inferred that the source of energy "pumping" the lines is the hard X-ray continuum. The simplest interpretation of Cyg X-3 assumes that the x-ray emission is from plasma in photoionization equilibrium.

To check or calibrate the models used to interpret these spectra, experimental data of photoionzied plasmas in relevant regimes are required. It was recognized recently that similar conditions of photoionized plasmas could be created in the laboratory using the intense burst of x-rays coming from the z-pinch at the SNLA Z-facility. [Heeter, 2001] An experiment was developed to measure the photoionized plasma x-ray spectra under

approximately scaled conditions. The figure of merit, the ionization parameter $\xi = L/n_e r^2$, where L, n_e, and r are the ionizing (x-ray) luminosity, electron density, and distance from the central source of ionizing radiation, resp., needs to be large, $\xi \geq 100$, to be relevant to astrophysical photoionized plasmas. This implies radiation dominance in the excitation and de-excitation processes.

The experiments were performed at the Sandia National Laboratory *Z* facility. The radiation from the pinch was generated by coupling a 20 MA, 100 ns rise time current pulse into a 2 cm diameter, 1 cm length, cylindrical wire array, creating a 8 ns FWHM, 120 TW, T_r = 165 eV near-blackbody radiation source. The sample charge state distribution, the absolute radiative flux, and the sample densities were measured independently. A typical spectrum from an Fe sample, located a distance of 1.5 - 1.6 cm from the pinch, is shown in Fig. 4c. [Foord, 2004] In this experiment, ξ reaches a value near 25 erg·cm/s at the peak of the radiation pulse, close to the desired values of 10^2-10^3 to resemble those of an accreting black hole.

A number of photoionized plasma models have now been compared with this laboratory experiment. Comparison of the predicted versus experimentally observed ionization distribution for an iron plasma is shown in Fig. 4d. [Rose, 2004] A radiation temperature of T_r = 165 eV, electron temperature of T_e = 150 eV and electron number density of $n_e = 2 \times 10^{19}$ cm^{-3} [Foord et al 2004] were assumed for the calculations with the average-atom model NIMP. Calculations are shown with and without including the radiation field. The observed ionization state would be underpredicted without the inclusion of the radiation field, which is a central feature of astrophysical photoionized plasmas. Also included in the comparison are predictions from the more detailed model

GALAXY presented for the same conditions. Good agreement with experiment is found only for the calculations that include the radiation field, but collisional effects are not completely negligible. The average-atom model is observed to be quite effective at calculating these photoionized plasma x-ray spectra, which is an important conclusion, because of its wide use in modeling laboratory plasmas.

Many astrophysical phenomena involve relativistic effects in collisionless plasmas. One example includes the Weibel instability, as it is thought to affect the observables from gamma ray bursts (GRB), illustrated schematically in Fig. 5a. [Medvedev, 1999] Due to the reflection of charged particles off the shock, launched by the GRB explosion, there exist counter-streaming plasmas. Fluctuations in current density lead to fluctuations in magnetic field distribution laterally, which interact with the counter-streaming currents, to cause filamentation, via this Weibel mechanism. [Medvedev, 1999] Laboratory experiments using ultraintense lasers see a similar effect. Here, the counter-propagating currents are due to a different source. In the intense laser-matter interactions, a relativistic, forward directed spray of relativistic electrons moves through the plasma. Space charge buildup causes a cooler return current to be set up. The net result is again counter-propagating currents, which can trigger the Weibel instability. Evidence has been observed experimentally, as shown in Fig. 5b, and PIC simulations has seen evidence for Weibel, as shown in Fig. 5c. [Wei, 2004] It seems possible that experiments of this nature could be configured to test aspects of the dynamics being modeled in GRB shocks, hence, a consideration of scaling is beneficial.

Figures 5d and 5e show the situation being considered, and the equations that apply to this relativistic, collisionless plasma regime are the Maxwell-Vlasov equations.

[Ryutov, 2007] Off-normal filamentary electron beam from two laser beam experiments. Image shows a typical electron filamented beam recorded on a RCF layer at the depth of 1240 μm in the rear stack.

The full set of the Maxwell-Vlasov equations describing collisionless plasmas, with relativistic electrons and non-relativistic ions was reduced to the dimensionless form in Refs. [Ryutov, 2006a; 2006b]. It was shown that, under the conditions described above, the system is fully characterized by the following six parameters:

$$n, L, \tau, \omega, E_0, M/Z, \tag{4}$$

which are: the particle density at a characteristic point of the blow-off plasma; length-scale (e.g., spot size) of the incident beam and the blow-off plasma; the pulse duration τ of the main pulse; the frequency ω of the incident radiation; the maximum amplitude E_0 of the electric field of the incident wave (or, equivalently, the maximum intensity I), and the mass-to-charge ratio for the accelerated ions. [The latter parameter may be of interest in the context of comparing the acceleration of hydrogen *vs*. deuterium.]

The dimensionless parameters that determine the scalability between any two (or more) systems are [13, 14]:

$$T \equiv \omega\tau;\ R \equiv L\omega/c;\ S \equiv \frac{4\pi n_0 ec}{E_0\omega};\ U \equiv \sqrt{\frac{ZeE_0}{M\omega c}}. \tag{5}$$

They must be held constant in order that the dimensionless equations remain unchanged between the two systems such that the evolution of these systems is similar.

In addition to holding the dimensionless parameters (5) constant, in order that the two systems behave in a scaled fashion, the geometric similarities must also be observed, e.g., if the characteristic length-scale L of the plasma density distribution is increased by

a factor of 2, so too must the focal spot radius be increased by the same factor. The geometrical characteristics of the incident radiation have to be identical between the two systems (up to the length-scale change): the polarization must remain the same, as well as the direction and the convergence of the incident beam. The shape of the temporal dependence of the laser pulse must also remain unchanged (although its duration may change). Under such conditions, any systems for which the dimensionless parameters (5) are kept the same, behave identically, up to scale transformations identified in Ref. [Ryutov, 2006a; 2006b]. Here we discuss, at a conceptual level, the possible experimental verification of the underlying physics assumptions, of which the most important are the absence of collisions and smallness of the initial "temperature." Within these two assumptions, the similarity covers all the processes involved, in all their complexity: distribution functions, the spatio-temporal characteristics of the reflected waves, possible presence of the filamentation and other instabilities, magnetic field generation, and so on.

Any observed differences may signify that either the basic assumptions are wrong (e.g., the system is actually collisional), or the two experiments are not perfectly similar in terms of their geometry (including the irradiation geometry), or the temporal dependence of the incident radiation.

We have six input parameters (Eq. (4)) subject to four constraints S=const, R=const, T=const, and U= const (Eq. (5)). To check the validity of scaling laws, we can arbitrarily choose any two of six input parameters in the primed system, then adjust the remaining four so as to keep the dimensionless parameters (Eq. (5)) constant. Consider,

VI. OUTLOOK FOR THE FUTURE

Looking ahead, there will be unique regimes of HED laboratory astrophysics that will become accessible on the NIF laser, under construction in the U.S. [Hogan, 2001], and the LMJ laser under construction in France. [Andre, 1999] The key scientific uncertainties in hydrogen relative to planetary interiors are at pressures greater than 1 Mbar, and along a quasi-isentrope. With the NIF and LMJ lasers, quasi-isentropic compression of hydrogen and H-He mixtures to pressures considerably greater than 1 Mbar should be possible, allowing tests of high pressure EOS models under conditions most relevant to the interiors of the giant planets.

In the studies of supernova explosion hydrodynamics, the key issues to examine are, in scaled divergent geometry, an experiment that evolves fully into the turbulent regime, in a diagnosable configuration. With the large energies and pointing flexibility of the NIF and LMJ lasers, such a scaled supernova hydrodynamics experiment should be both possible and diagnosable. This would help answer whether the "standard model" of core collapse supernovae is able to reproduce the astronomically observed rapid core inversions.

One of the key issues in protostellar jet dynamics is how high Mach number, radiatively cooled jets stay collimated, and under what conditions they do or do not become turbulent, in their interactions with the interstellar medium (ISM). Scaled jet experiments on the NIF and LMJ lasers should be able to evolve deeply into regimes where turbulence should be expected, and thereby help answer questions relevant to the collimation of protostellar jets.

To study scaled systems relevant to compact object (neutron stars, black holes)

accretion disks requires a low density, radiation dominated, photoionized plasma. An exceedingly high flux of thermal x-rays is needed so that, in the surrounding plasma, atomic excitations, ionization, and recombination processes are dominated by the radiation field, with the effects from electron-ion collisions being negligible. On NIF and LMJ, creating these intense x-ray luminosities should be possible, allowing models of photoionized plasmas, relevant to accreting black holes, to be checked and calibrated, in a properly scaled experimental testbed.

In conclusion, exceptional progress has been made over the past decade on developing the new field of HED laboratory astrophysics, as is evident by the breadth and depth of results being reported in literature. [HEDLA-2004, 2005] With the construction of the NIF and LMJ lasers, the next decade should witness several breakthroughs in understanding of energetic astrophysical processes, aided by scaled HED laboratory experiments.

ACKNOWLEDGEMENTS

*The work was performed out under the auspices of the U.S. Department of Energy by Lawrence Livermore National Laboratory under Contract DE-AC52-07NA27344.

REFERENCES

[Andre, 1999] M.L. Andre, Fusion Engineering and Design 44: 43-49 FEB 1999.

[Bailey, 2007] J.E. Bailey et al., PRL (2007).

[Belov, 2002] S.I. Belov et al., Pis'ma Zh. Eksp. Teor. Fiz. 76, 508 (2002) [English version: JETP Lett. 76, 433 [2002)].

[Benuzzi-Mounaix, 2002] A. Benuzzi-Mounaix et al.., Phys. Plasmas 9, 2466 (2002).

[Blondin, 1990] J. Blondin et al., Ap. J. 360, 370 (1990).

[Boehly, 2004] T. Boehly et al., Phys. Plasmas 11, L49 (2004).

[Bouquet, 2000] S. Bouquet et al., Ap. J. Suppl. 127, 245 (2000).

[Bouquet, 2004] S. Bouquet et al., Phys. Rev. Lett. 92, 225001 (2004).

[Boriskov, 2003] G.V. Boriskov et al., Dokl. Akad. Nauk 392, 755 (2003) [English version: Dokl. Phys. 48, 553 (2003).

[Celliers, 2004] P.M. Celliers et al., Phys. Plasmas 11, L41 (2004).

[Collins, 1998] G.W. Collins et al., Science 281, 1178 (1998).

[Courtois, 2004] C. Courtois, R.A.D. Grundy, A.D. Ash, D.M. Chambers, N.C. Woolsey, R.O. Dendy, K.G. McClements , Physics of Plasmas. 11, 3386-3393 (2004).

[Courtois, 2005] C. Courtois, R.A.D. grundy, A.D. Ash, D.M. Chambers, and N.C. Woolsey, R.O. Dendy, and K.G. McClements, in press, Astrophys. Space Science (July, 1995).

[Cowan, 1999] T.E. Cowan, M.D. Perry, M.H. Key, T.R. Ditmire, S.P. Hatchett, E.A. Henry, J.D. Moody, M.J. Moran, D.M. Pennington, T.W. Phillips, T.C. Sangster, J.A. Sefcik, M.S. Singh, R.A. Snavely, M.A. Stoyer, S.C. Wilks, P.E. Young, Y. Takahashi, B. Dong, W. Fountain, T. Parnell, J. Johnson, A.W. Hunt, T. Kuhl, Laser and Particle Beams **17**, 773-783 (1999).

[Cowan, 2000] T.E. Cowan, M. Roth, J.Johnson, C.Brown, M.Christl, W. Fountain, S. Hatchett, E.A. Henry , AW. Hunt, MH. Key, A. MacKinnon, T.Parnell, DM.Pennington, MD. Perry, TW. Phillips , TC. Sangster, M. Singh, R. Snavely, M. Stoyer, Y. Takahashi, SC.Wilks , K. Yasuike, Nuclear Instruments & Methods in

Physics Research Section A-Accelerators Spectrometers Detectors & Associated Equipment 455, 130-139 (2000).

[Da Silva, 1992] Da Silva et al., PRL 69, 438 (1992)]

[Drake, 2002] R.P. Drake, Phys. Plasmas **9**, 727-728 (2002).

[Dziewonski, 1981] Dziewonski, A. M., and Anderson, D. L., Phys. Earth Planet. Inter., 25, 297 (1981).

[Edwards, 2001] J. Edwards et al., Phys. Rev. Lett. 87, 085004 (2001).

[Ferrarese, 1996] Ferrarese et al., Ap. J. 470, 444 (1996).

[Fleury, 2002] X. Fleury et al., Laser and Particle Beams 20, 263 (2002).

[Foord, 2004] M.E. Foord et al., Phys. Rev. Lett. 93,, 055002 (2004).

[Fortney, 2004] J.J. Fortney and W.B. Hubbard, Åp. J. 608, 1039 (2004).

[Foster, 2002] J. Foster et al., Phys. Plasmas 9, 2251 (2002).

[Guillot, 1999] T. Guillot, Science 286, 72 (1999).

[Hansen, 2004] J.F. Hansen et al., submitted, Phys. Rev. Lett. (2004).

[Hatchett, 2000] Hatchett, S.P., C.G. Brown, T.E. Cowan, E.A. Henry, J.S. Johnson, M.H. Key, J.A. Koch, A.B. Langdon, B.F. Lasinski, R.W. Lee, A.J. Mackinnon, D.M. Pennington, M.D. Perry, T.W. Phillips, M. Roth, T.C. Sangster, M.S. Singh, R.A. Snavely, M.A. Stoyer, S.C. Wilks, and K. Yasuike, Phys. Plasmas 7, 2076-2082 (2000).

[HEDLA-2004, 2005] Proceedings of the 5th International Conference on High Energy Density Laboratory Astrophysics, in press, Astrophys. Space Science 298:1-2 (July 2005).

[Heeter, 2001] R.F. Heeter et al., Rev. Sci. Instrum. 72, 1224 (2001).

[Hogan, 2001] W.J. Hogan et al., Nuclear Fusion 41, 567 (2001).

[Holmes, 1995] N. Holmes et al.,PRB 52, 15835 (1995).

[Hubbard, 1997] W.B. Hubbard, Science 275, Issue 5304, 1279 (1997).

[Kane, 1999] J. Kane et al., Phys. Plasmas 6, 2065 (1999).

[Keilty, 2000] K.A. Keilty et al., Ap. J. 538, 645 (2000).

[Keiter, 2002] P.A. Keiter et al., Phys. Rev. Lett. 89, 165003 (2002).

[Key, 1999] Key, M.H. M.D. Cable, T.E. Cowan, K.G. Estabrook, B.A. Hammel, S.P. Hatchett, E.A. Henry, D.E. Hinkel, J.D. Kilkenny, J.A. Koch, W.L. Kruer, A.B. Langdon, B.F. Lasinski, R.W. Lee, B.J. MacGowan, A.J. MacKinnon, J.D. Moody, M.J. Moran, A.A. Offenberser, D.M. Pennington, M.D. Perry, T.J. Phillips, T.C. Sangster, M.S. Singh, M.A. Stoyer, Phys. Plasmas **5**, 1966-1972 (1998).

[Kifonidis, 2000] Kifonidis et al., Ap. J. 531, L123 (2000).

[Knudson, 2003] M.D. Knudson et al., PRL 90, 035505 (2003).

[Koenig, 2004] M. Koenig et al., Nuclear Fusion, in press (2004).

[Koenig, 2000] M. Koenig et al., Recherche 330, 46 (2000).

[Lasinski, 1999] Barbara F. Lasinski, A. Bruce Langdon, Stephen P. Hatchett, Michael H. Key, and Max Tabak, Phys. Plasmas 6, 2041 (1999).

[Lebedev, 2002] S. Lebedev et al., Ap.J. 564, 113 (2002).

[Liang, 1998] Liang, E.P., S.C. Wilks, M. Tabak, Phys. Rev. Lett. 81, 4887-4890 (1998).

[Liang, 2003] Liang, E., Nishimura, K. Li, H. and Gary, S.P., Phys. Rev. Lett. 90, 085001 (2003).

[Libby, 2004] S.B. Libby, M. Tabak, R.D. Hoffman, M.A. Stoyer, S.W. Haan, S.P. Hatchett, D.P. NcNabb, W.E. Ormand, J. Escher, P. Navratil, D. Gogny, M.S. Weiss,

M. Mustafa, J. Becker, W. Younes, E. Hartouni, and R.A. Ward, proceedings of IFSA-2003, Ed. B.A. Hammel, D.D. Meyerhofer, J. Meyher-ter-Vehn, and H. Azechi, (American Nuclear Society, Inc, La Grange Park, IL, 2004), 935-939 (2004).

[Liedahl, 1996] D.A. Liedahl and F. Paerels, Ap. J. 468, L33 (1996).

[Medvedev, 1999] Medvedev & Loeb, Ap.J. 526, 697 (1999).

[Meszaros, 1993] P. Mészáros, P. Laguna, M.J. Rees, Astrophys. J. 415, 181-190 (1993).

[Meszaros, 2000] P. Mészáros, Nuclear Physics B-Proceedings Suppl. 80, 63-77 (2000).

[Michaut, 2004a] C. Michaut et al., IFSA-2003 proceedings (2004).

[Michaut, 2004b] C. Michaut et al., Eur. Phys. J. D 28, 381 (2004).

[Miles, 2004] A. Miles *et al.,* PoP 11, 3631 (2004).

[Moon, 2005] S. Moon, S. Wilks, R. Klein, H. Chen, J. Kuba, A. MacKinnon, P. Patel, B. Remington, D. Ryutov, R. Shepherd, A. Spitkovsky, and R. Town, in press, Astrophys, Space Science Vol. 298, No. 1-2 (July, 2005). [Mostovych, 2001] A.N. Mostovych et al., Phys. Plasmas 8, 2281 (2001).

[Nellis, 2002] W.J. Nellis et al., Phys. Rev. Lett. 89, 165502 (2002).

[Nguyen, 2004] J.H. Nguyen and N.C. Holmes, Nature 427, 339 (2004).

[Piner, 2001] B. Glenn Piner, Dayton L. Jones, and Ann E. Wehrle, Astron. J., 122, 2954-2960 (2001).

[Reighard, 2004] A.B. Reighard et al., submitted, Phys. Rev. Lett. (2004).

[Reipurth, 2001] B. Reipurth and Bally, Ann. Rev. Astron. Astrophys. 39, 403 (2001).

[Remington, 1999] B.A. Remington et al., Science 284, 1488 (1999).

[Remington, 2000] B.A. Remington et al., Phys. Plasmas 7, 1641 (2000).

[Rogers, 1994] F. Rogers and C. Iglesias, Science 263, 50 (1994).

[Rose, 2004] S.J. Rose et al., J. Phys. B: At. Mol. Opt. Phys. 37, L337 (2004).

[Rose, 2005] S.J. Rose, private communication (2005).

[Ryutov, 1999] D.D. Ryutov et al., Ap. J. 518, 821 (1999).

[Ryutov, 2000] D.D. Ryutov et al., Ap. J. Supple. 127, 465 (2000).

[Ryutov, 2001] D.D. Ryutov et al., Phys. Plasmas 8, 1804 (2001).

[Ryutov, 2006a] D.D. Ryutov, B.A. Remington. "Optimizing laboratory experiments for dynamic astrophysical phenomena." Paper presented at 3rd Intern. Conf. on Superstrong Fields in Plasmas, Varenna, Sept. 19-24 2005 (To appear in AIP Proceedings, April 2006).

[Ryutov, 2006b] D.D. Ryutov, B.A. Remington. Plasma Phys. Contr. Fus., 48, L23-L31 (2006).

[Ryutov, 2007] D.D. Ryutov et al., ApSS 307, 291 (2007).

[Saumon, 2004] D. Saumon and T. Guillot, Ap.J. 609,1170 (2004).

[Snavely, 2000] Snavely, R.A., M.H. Key, S.P. Hatchett, T.E. Cowan, M. Roth, T.W. Phillips, M.A. Stoyer, E.A. Henry, T.C. Sangster, M.S. Singh, S.C. Wilks, A.J. Mackinnon, A. Offenberger, D.M. Pennington K. Yasuike, A.B. Langdon, B.F. Lasinski, J.S. Johnson, M.D. Perry, E.M. Campbell, Phys. Rev. Lett. **85**, 2945-2948 (2000).

[Takabe, 2001] H. Takabe, Progress of Theoretical Physics Supplement 143, 202-265 (2001).

[Tatarikis, 1998] Tatarakis, M., J.R. Davies, P. Lee, P.A. Norreys, N.G. Kassapakis, F.N. Beg, A.R. Bell, M.G. Haines, A.E. Dangor, Phys. Rev. Lett. **81**, 999-1002 (1998).

[Tatarikis, 2002a] Tatarakis M., A. Gopal, I. Watts, F.N. Beg, A.E. Dangor, K. Krushelnick, U. Wagner, P.A. Norreys, E.L. Clark, M. Zepf, R.G. Evans, Phys. Plasmas **9**, 2244-2250 (2002a).

[Tatarikis, 2002b] Tatarakis M., A. Gopal, I. Watts, F.N. Beg, A.E. Dangor, K. Krushelnick, U. Wagner, P.A. Norreys, E.L. Clark, M. Zepf, R.G. Evans, Phys. Plasmas **9**, 3642 (2002b).

[Tatarikis, 2002c] Tatarakis, M., I. Watts, F.N. Beg, E.L. Clark, A.E. Dangor, A. Gopal, M.G. Haines, P.A. Norreys, U. Wagner, M.S. Wei, M. Zepf, K. Krushelnick, Nature **415**, 280-280 (2002c).

[Urry, 2000] Urry, C.M., 2000, in: Cosmic Explosions, Proc. 10th Astrophysics Conference, College Park, Maryland, AIP Conf. Proc. 522, 299-306 (1999).

[Van Horn, 1991] H.M. Van Horn, Science 252, 384 (1991).

[Valencia, 2007] Valencia et al., Ap. J. 656, 545 (2007).

[Wei, 2004] Wei et al., PRE 70, 056412 (2004).

[Wilks, 2001] Wilks, S.C., A.B. Langdon, T.E. Cowan, M. Roth, M. Singh, S. Hatchett, M.H. Key, D. Pennington, A. MacKinnon, and R.A. Snavely, Phys. Plasmas **8**, 542-549 (2001).

[Woolsey, 2001] N.C. Woolsey, Y.A. Ali, R.G. Evans, R.A.D. Grundy, S.J. Pestehe, P.G. Carolan, N.J. Conway, R.O. Dendy, P. Helander, K.G. McClements, J.G. Kirk, P.A. Norreys, M.M. Notley, and S.J. Rose, Phys. Plasmas, 8, 2439-2445 (2001).

[Woolsey, 2002] N. C. Woolsey, Y. Abou Ali, R. G. Evans, R. A. D. Grundy, and S. J. Pestehe, P. G. Carolan, N. J. Conway, R. O. Dendy, P. Helander, and K. G. McClements, J. G. Kirk, P. A. Norreys, M. M. Notley, and S. J. Rose, Phys. Plasmas 9, 729-730 (2002).

[Woolsey, 2004] N C Woolsey et al, PPCF 46, B397 (2004).

FIGURE CAPTIONS

Fig. 1. Stellar interiors and opacity measurements. (a) Diagram of the ratio of the first two harmonics periods of a beat Cepheid variable star. Circles represent observations. The upper set of three dashed curves correspond to the simulated result using older opacities, which ignore the full fine structure of the metals. The lower solid curves correspond to simulations with OPAL-DTA, including the full fine structure, in particular, for Fe. [Adapted from Rogers and Iglesias, 1994.] (b) Schematic showing approximately the density and temperature of the interior of the sun, as a function of the normalized radius. [Rose, 2005] (c) Schematic experiment diagram for the Fe opacity experiment done on the Z facility. Example space-resolved "raw" spectra from one of the Z experiments are shown above the diagrams. [Bailey, 2007] (d) Iron opacity calculated at the radiation- convection boundary in the sun (red) and at the conditions in Z experiments (green). The Planck function derivative with respect to temperature evaluated at 182 eV (black) illustrates the photon energies most important for the solar radiation transport. [Bailey, 2007]

Fig. 2. (a) Schematic of the interior of Jupiter, reproduced from [Guillot, 2004]. (b) Internal structure of GJ 876d: density profile. Four different compositions are illustrated. The surface is to the right and the center of the planet is to the left. The solid lines show the cases in which the composition of the core is taken to be pure Fe; dashed lines are for the case of $Fe_{0.2}(FeS)_{0.8}$. Lines with stars show the internal structure of GJ 876d if the composition is Earth-like. Squares show the density profile if this planet has 80% of the mass in the core. Circles show the structure if the planet had retained 20% of its mass as a water /ice layer. Diamonds show the density structure if GJ 876d retained 40% of water /ice. The Preliminary Reference Earth Model [PREM; Dziewonski & Anderson 1981] is shown for reference. [Valencia, 2007] (c) Shock-free loading of aluminum to 200 GPa in an experiment developed on the Omega laser. Particle velocity (lower curve) at the Al-LiF interface and extracted pressure (upper curve) at the front of the Al sample taken from the VISAR record in (a). Heavy solid lines show velocity and extracted pressure averaged over 300 μm. Shading shows error bars generated from a spatial analysis of six velocity records e one taken every 50 pixels. Shading represents 90% confidence limits for both particle velocity and pressure. Over the peak drive window (t = 20-30 ns), the average deviation in particle velocity and pressure are 3.6% and 5.5%, respectively. [Lorenz, 2006] (d) Quasi-isentropic stress versus density data presented here from the experiment on the Omega laser together with previous data from Davis. Also shown are Hugoniot and cold curve data, and a calculated isentrope from the 3700 EOS model from the Sesame database. The inset shows $C_L(u)$ for all seven shots. The black line represents the weighted mean hCLi for all shots with the analysis limited to times preceding the influence of the LiF shock or reverberations in the case of Al=vacuum targets. The gray dashed line represents the weighted mean over the entire profile. [Smith, 2007]

Fig. 3. (a) 2D simulation of SN 1987A, showing the RT instability induced spikes of core material impacting the reverse shock at the He-H interface, at three times: 100 s, 1500 s, and 20,000 s. Reproduced from [Kifonidis, 2006]. (b) Measurements of the nonlinear RT evolution of a preimposed perturbation, from the Omega experiment, at three time steps: 13, 25, and 37 ns. Reproduced from [Miles, 2004; Kuranz, 2005].

Fig. 4. (a) Images of the intergalactic jet, and the accretion disk around the active galactic nucleus, NGC 4261, reproduced from [Piner, 2001; Ferrarese, 1996]. (b) X-ray spectrum of the photoionized plasma in the immediate vicinity of Cyg X-3 x-ray binary, reproduced from [Liedahl, 1996]. (c) X-ray spectrum in a scaled experiment done on the Z pinch facility at SNLA, reproduced from [Foord, 2004]. (d) Photoionized plasma models of the ionization distribution observed in the Z photoionized plasma experiment, reproduced from [Rose, 2004].

Fig. 5. (a) Illustration of the instability. A magnetic field perturbation deflects electron motion along the x-axis, and results in current sheets (j) of opposite signs in regions I and II, which in turn amplify the perturbation. The amplified field lies in the plane perpendicular to the original electron motion. [Reproduced from Medvedev, 1999] (b) Off-normal filamentary electron beam from two laser beam experiments. Image shows a typical electron filamented beam recorded on a RCF layer at the depth of 1240 μm in the rear stack. [Reproduced from Wei, 2004] (c) Simulation results of the structure of the time averaged quasistatic magnetic fields at 144 fs with different density scale lengths at the target rear surface. This case corresponds to a slow ramp from $20n_c$ to n_c within $14c / \omega_0$. Here x_1 is the coordinate along laser direction of propagation. A linearly polarized laser pulse with an intensity 10^{19} W / cm^2 is incident from the left boundary. The plasma and laser light are uniform in the x_2 direction. One unit in space corresponds to 0.16 μm. [Wei, 2004] (d) and (e) Scenario assumed in the the theoretical scale transformation of the Maxwell-Vlasov equations, discussed in the text. [Ryutov, 2007]

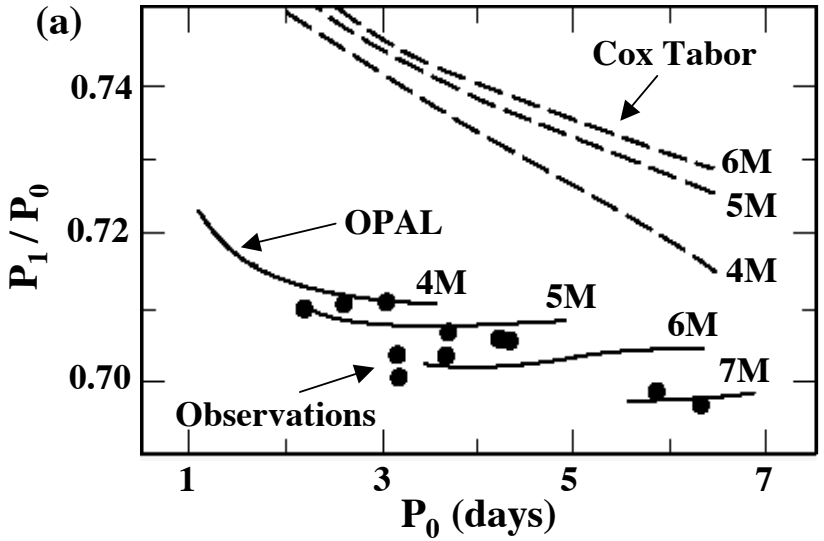

[Rogers & Iglesias, Science 263, 50 (1994);
Da Silva et al., PRL 69, 438 (1992)]

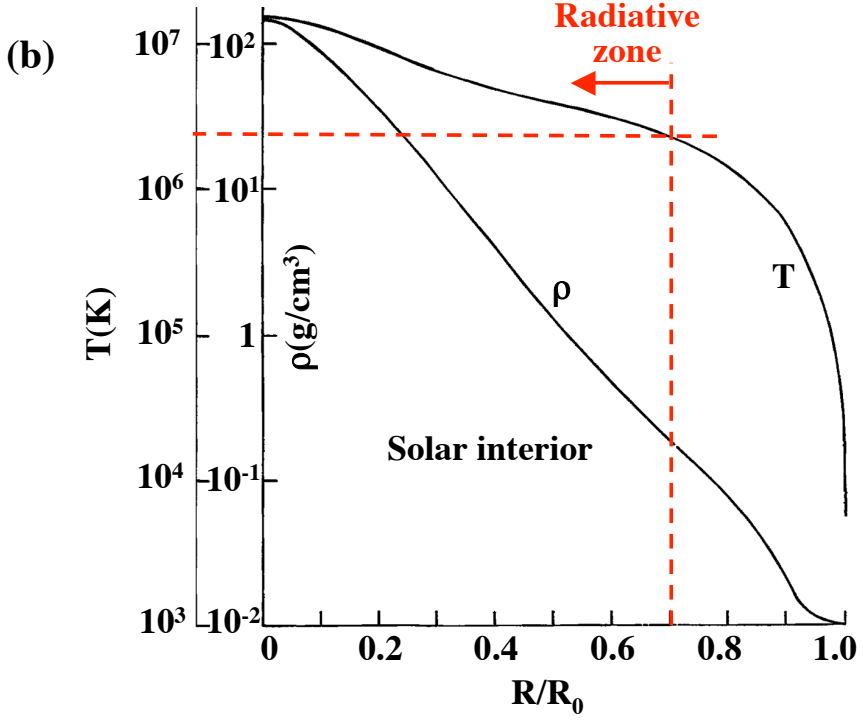

[Courtesy of Steve Rose (2005)]

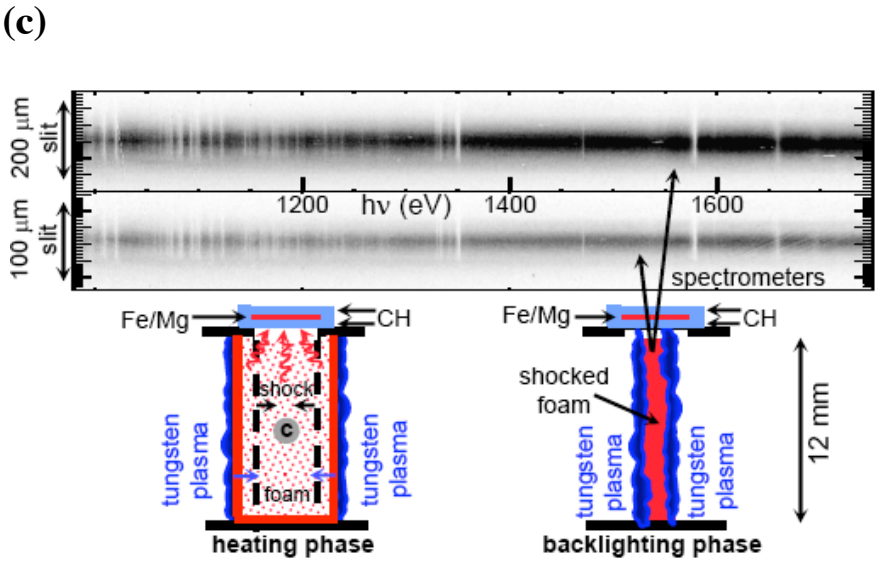

[J.E. Bailey et al., PRL (2007)]

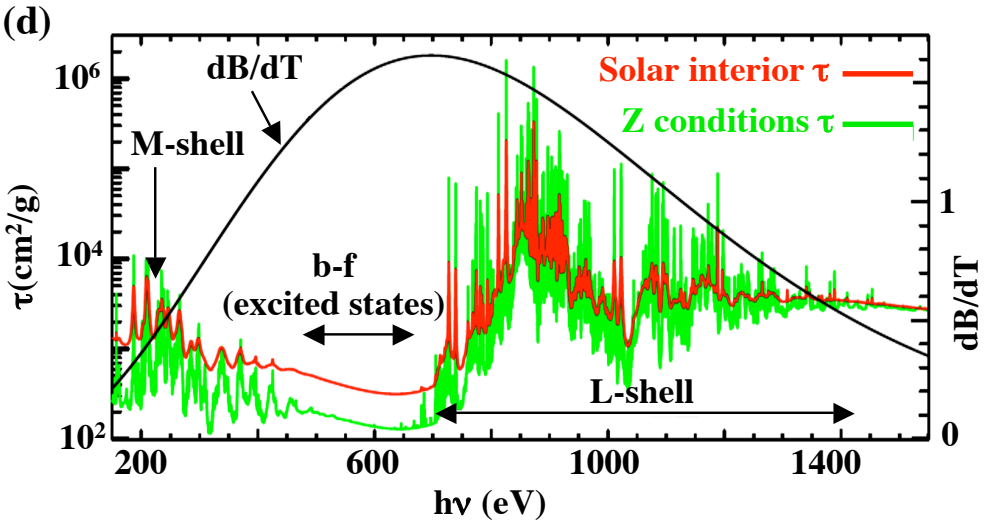

[J.E. Bailey et al., PRL (2007)]

Figure 1

(a)

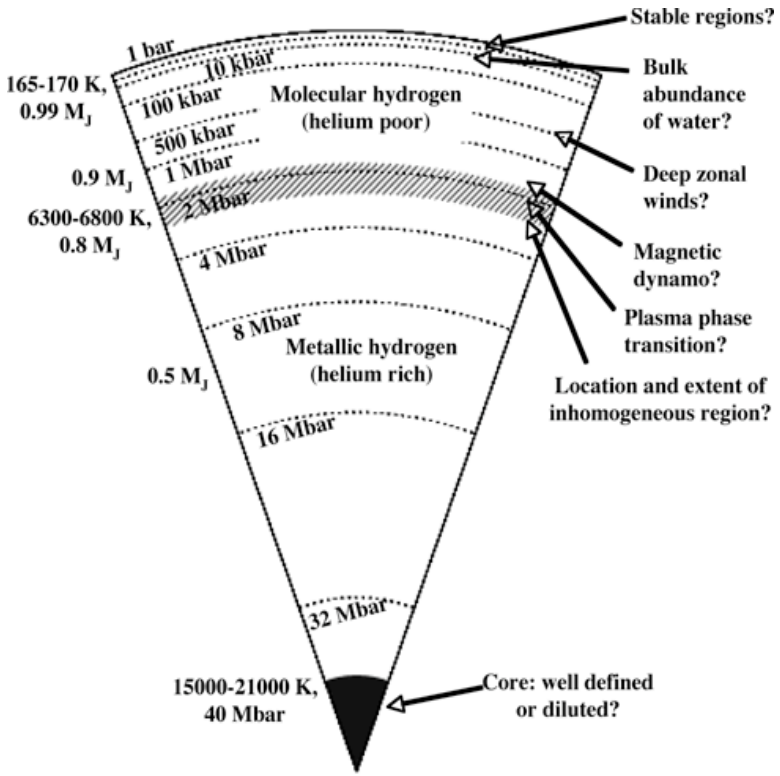

[Tristan Guillot, in *Jupiter* book (2004)]

(b)

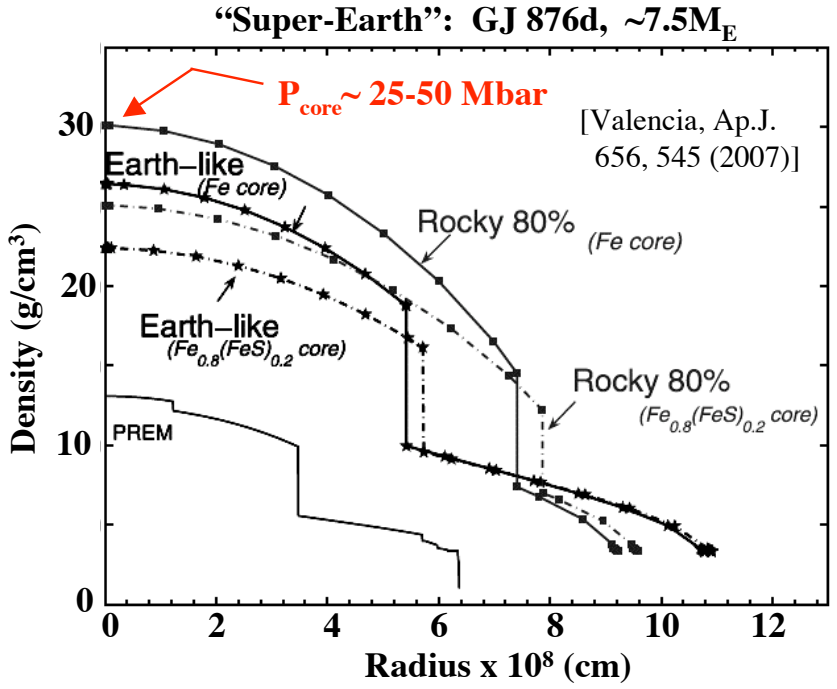

(c)

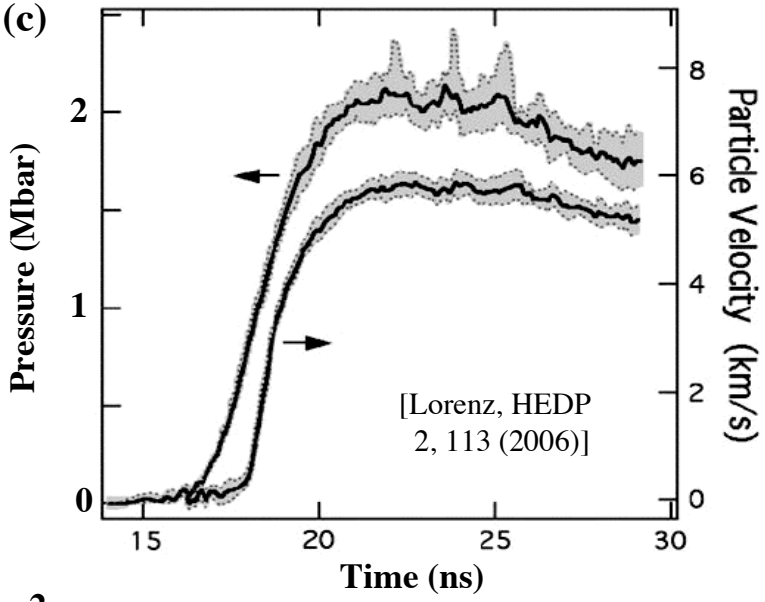

(d)

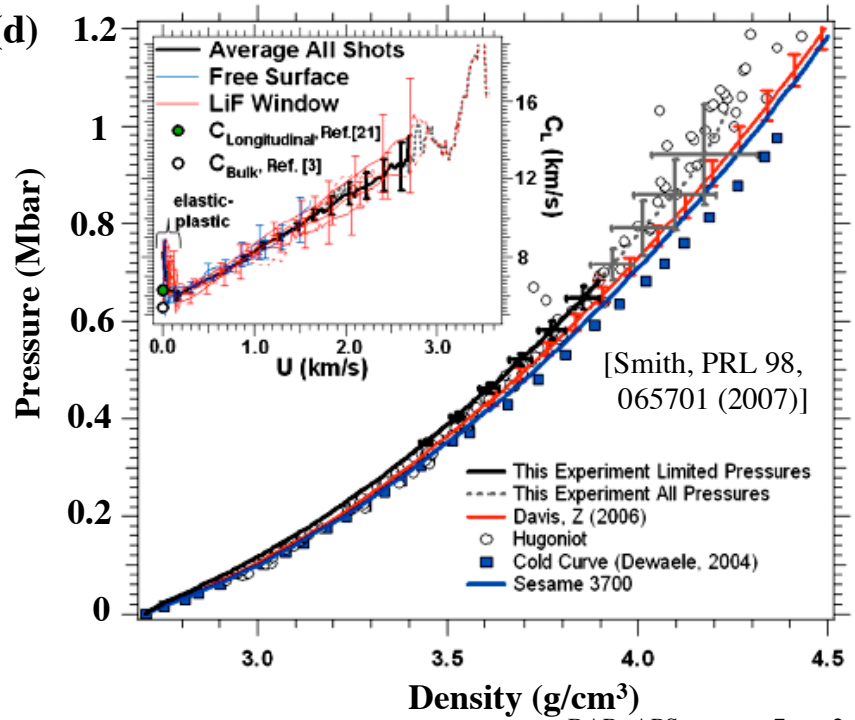

Figure 2

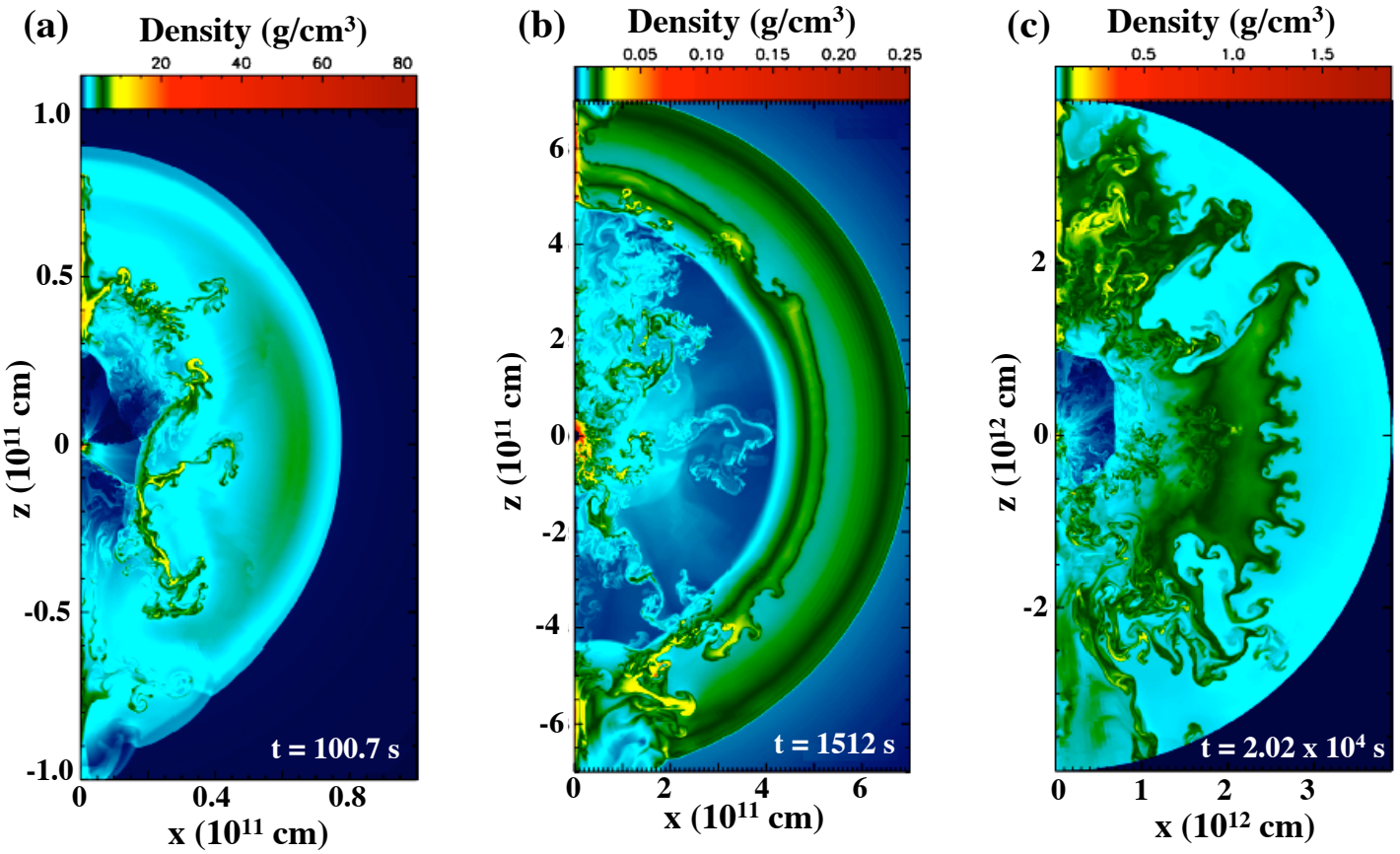

[Kifonidis *et al.,* AA. 453, 661 (2006)]

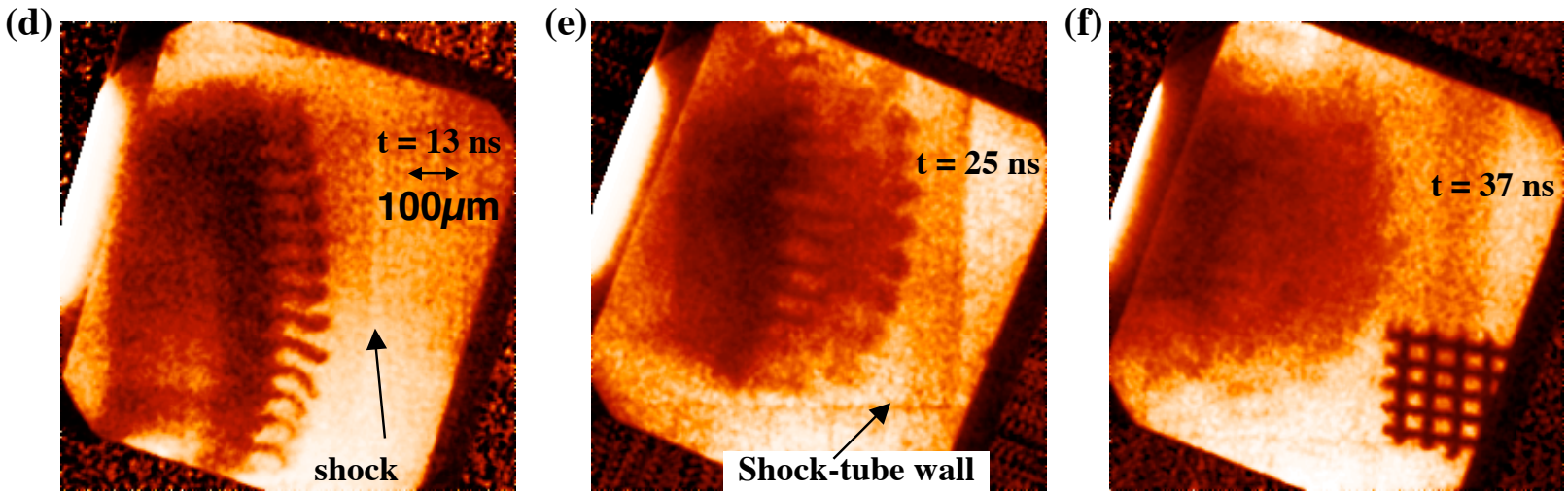

Figure 3

[C. Kuranz et al., ApSS 298, 9 (2005);A. Miles et al., PoP 12, 056317 (2005)]

(a)

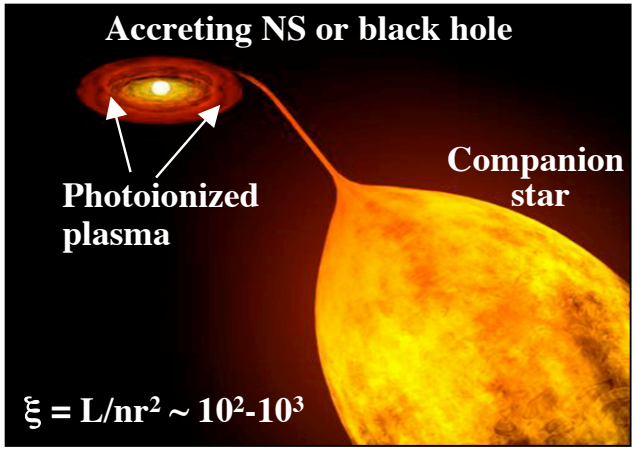

(b)

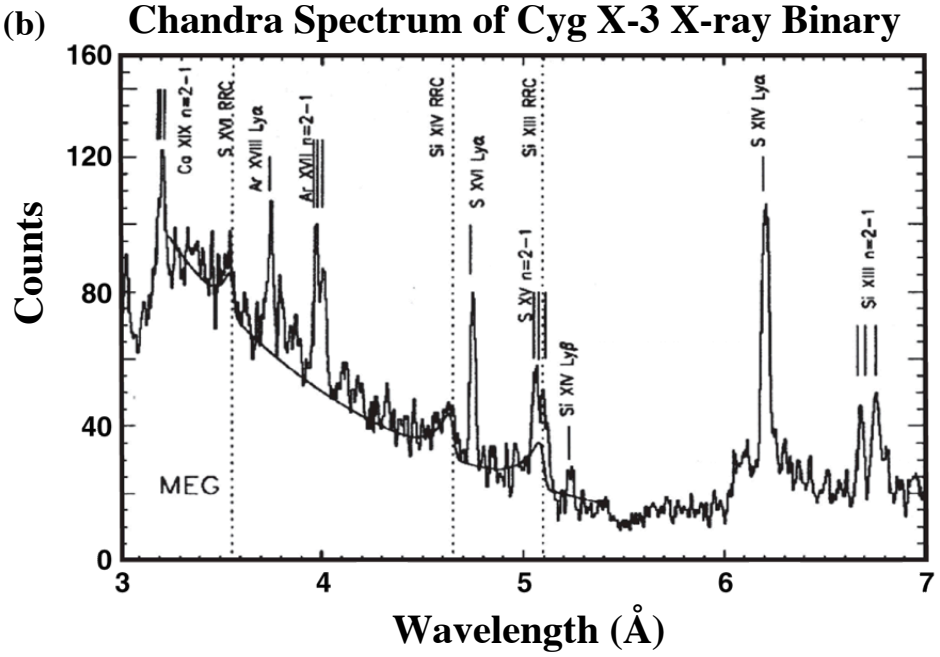

[Paerels, Ap.J.Lett. 533, L135 (2000)]

(c)

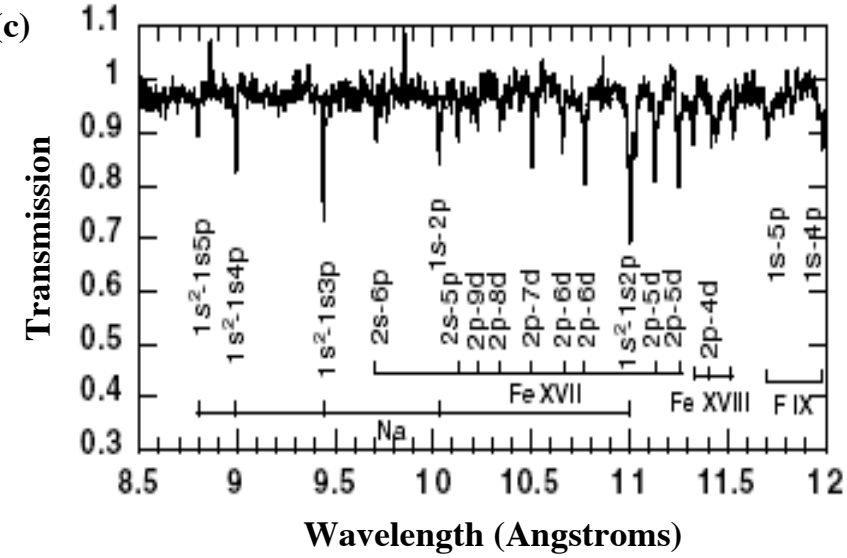

[Foord, PRL 93, 055002 (2004)]

(d)

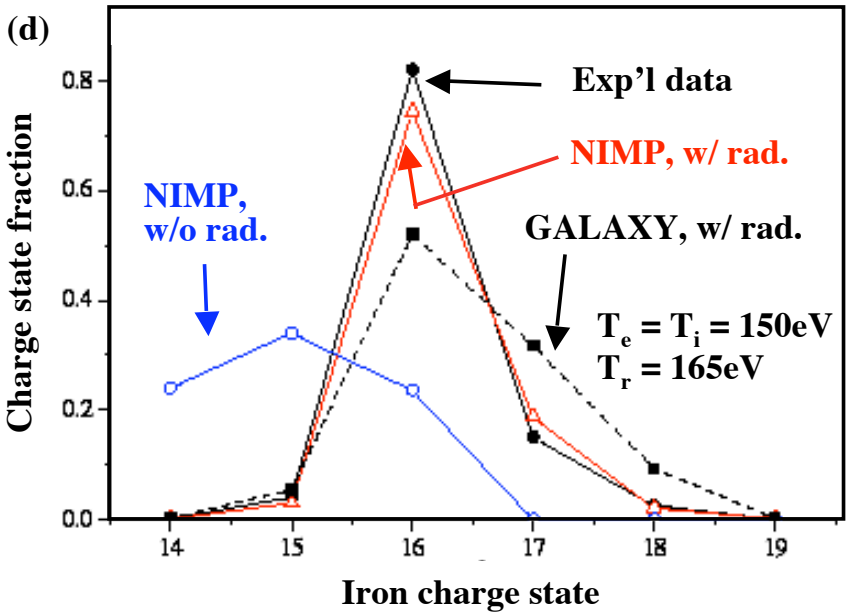

Figure 4

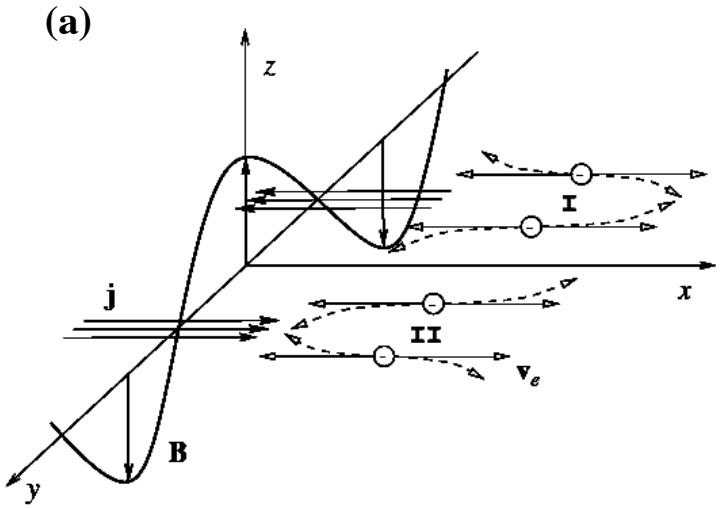

[Medvedev & Loeb, ApJ 526, 697 (1999)]

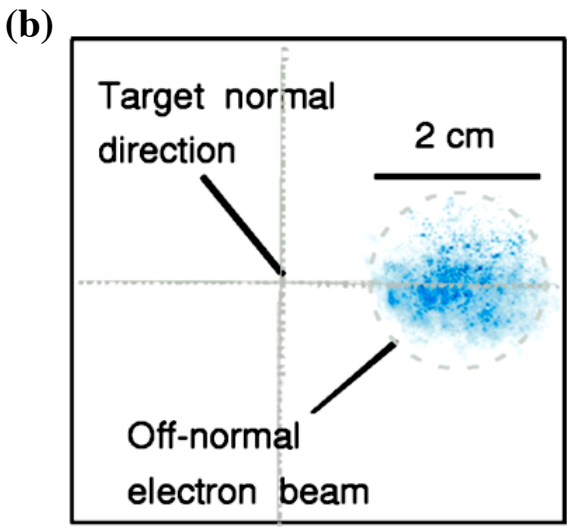

[Wei et al., PRE 70, 056412 (2004)]

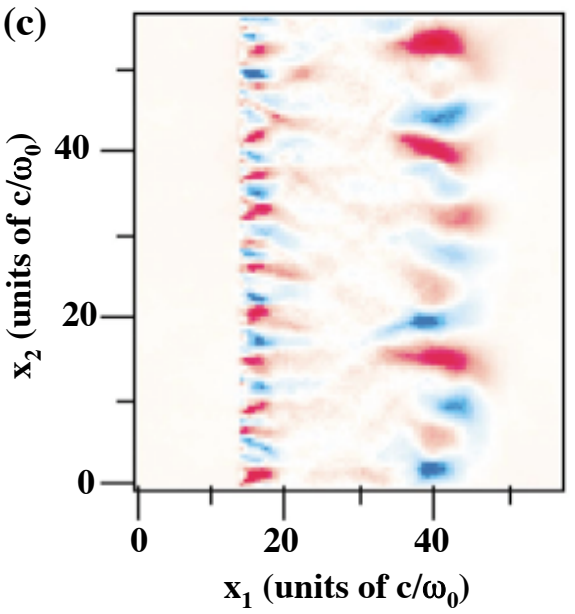

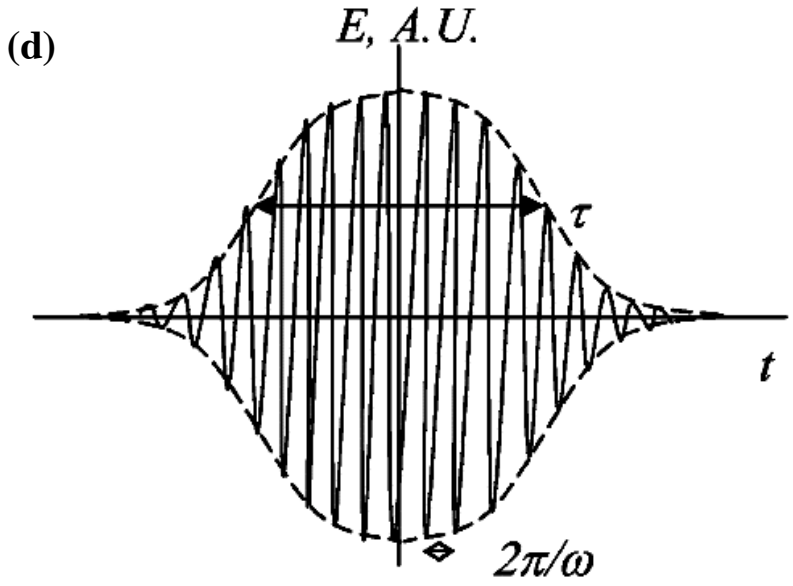

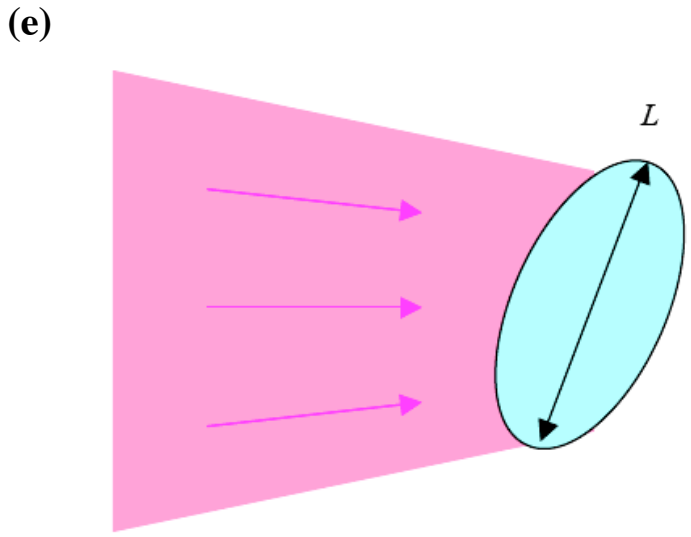

Figure 5

[Ryutov, ApSS 307, 291 (2007)]